Scripta Materialia 239 (2024) 115799

Contents lists available at ScienceDirect

Scripta Materialia

journal homepage: www.journals.elsevier.com/scripta-materialia

Skyrmions in van der Waals centrosymmetric materials with Dzyaloshinskii–Moriya interactions

Hung Ba Tran [a,b,*], Yu-ichiro Matsushita [a,b,c]

[a] Laboratory for Materials and Structures, Institute of Innovative Research, Tokyo Institute of Technology, Midori-ku, Yokohama 226-8503, Japan
[b] Quemix Inc., 2-11-2 Nihonbashi, Chuo-ku, Tokyo 103-0027, Japan
[c] Quantum Material and Applications Research Center, National Institutes for Quantum Science and Technology, 2-12-1, Ookayama, Meguro-ku, Tokyo 152-8552, Japan

ARTICLE INFO

Keywords:
Skyrmions and meron
Van der Waals centrosymmetric materials
Dzyaloshinskii–Moriya interactions
Magnetic phase diagram

ABSTRACT

Skyrmions can appear in non-centrosymmetric materials because of non-vanishing Dzyaloshinskii–Moriya interactions (DMIs). We investigate the magnetic properties of rhombohedral MX_3 (M: V, Cr, Mn, Fe; X: Cl, Br, I) van der Waals materials with centrosymmetric lattices by combining first-principle calculations and Monte Carlo simulations. We determine that the Dzyaloshinskii–Moriya vector acting between the second nearest neighbor sites of the intralayer is non-zero and large in MX_3, owing to the breaking of the local inversion symmetry. Large DMIs cause nanoscale magnetic vortices, i.e. that is, skyrmions. We observe both conventional skyrmions in $CrCl_3$ and VCl_3 and antiferromagnetic skyrmions in $FeCl_3$ and merons in $MnCl_3$. Furthermore, the skyrmions in $CrCl_3$ and VCl_3 have different helicities, indicating the possibility of controlling the helicity by electron/hole doping in MX_3 materials. Van der Waals materials have high degrees of freedom in heterostructures and twisted structures, demonstrating promising potential as skyrmion materials.

Skyrmions, which are small magnetic swirls, are promising for future spintronic applications such as race track memory devices [1,2]. Conventional skyrmions are known to exist in non-centrosymmetric materials owing to the antisymmetric exchange of the Dzyaloshinskii–Moriya interactions (DMIs) [1,2]. In centrosymmetric materials, the DMI is known to be zero, and it cannot support the appearance of skyrmions [3]. However, recent experimental studies have shown that skyrmions can be realized even in centrosymmetric materials such as triangular lattices [4–6]. This is because of the frustration or oscillation of the magnetic exchange coupling constant J_{ij}, which is also known as the Ruderman–Kittel–Kasuya–Yosida (RKKY) interaction [4–7]. The presence of a skyrmion in a centrosymmetric material offers several advantages; for example, the helicity and polarity can be controlled as additional degrees of freedom, which can be useful when developing future computing hardware such as skyrmion qubits in quantum computing or neuromorphic computing [7–11]. Thus, exploring other possible mechanisms to realize skyrmions in a new class of centrosymmetric materials is an important task for both theoretical and experimental frameworks.

Two dimensional (2D) materials, such as heterostructures and twisted structures, have a high degree of structural freedom and offer an interesting premise for the development of future electronic devices and observation of new physics phenomena, e.g.for example, superconductivity and Fermi velocity modulation in twisted bilayer graphene [12–19]. Van der Waals magnetic 2D materials such as the ferromagnetic 2D materials CrI_3 and their family have attracted considerable attention owing to their peculiar properties arising from their layered structure. This makes it possible to manufacture a few layers or even a monolayer with some certain new physical properties, such as spin flip and peculiar magnetoresistance properties, rather than manufacturing bulk systems [12,13,20]. Bulk CrI_3 has two crystal structures: a low-temperature rhombohedral phase with space group $R\bar{3}$ and a high-temperature monoclinic phase with space group $C2/m$ [21]. The low-temperature crystal structure of CrI_3 ($R\bar{3}$) is shown in Fig. 1a. The crystal structure is centrosymmetric with a honeycomb lattice, which leads to the DMI being ignored. The *ab* plane of CrI_3 with two sublattices is shown in Fig. 1b. The second nearest neighbor of the intralayer has a broken local inversion symmetry, where the center of this pair does not satisfy inversion symmetry. This indicates the possibility of a

* Corresponding author at: Laboratory for Materials and Structures, Institute of Innovative Research, Tokyo Institute of Technology, Midori-ku, Yokohama 226-8503, Japan.
E-mail address: tran.h.ag@m.titech.ac.jp (H.B. Tran).

https://doi.org/10.1016/j.scriptamat.2023.115799
Received 1 June 2023; Received in revised form 25 July 2023; Accepted 28 September 2023
Available online 10 October 2023

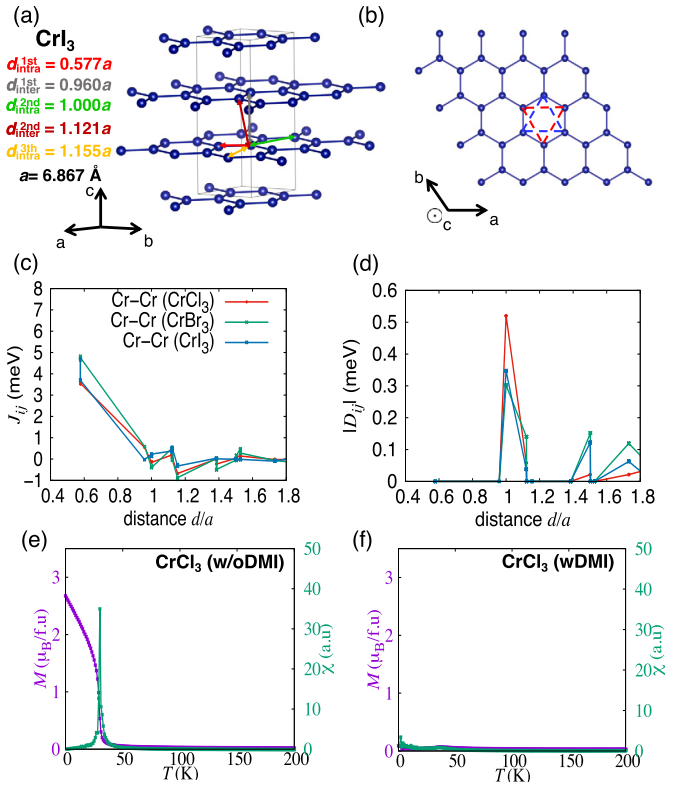

Fig. 1. (**a**) Crystal structure of rhombohedral CrI_3, where the only Cr atom is shown as a blue sphere. (**b**) Layer of honeycomb lattice, where two sublattices of the second nearest neighbor of the intralayer are indicated as red and blue dashed lines. (**c**) Magnetic exchange coupling constants of Cr–Cr pairs of CrX_3 (X: Cl, Br, I) as a function of the distance over the lattice constant (d/a). (**d**) Length of the Dzyaloshinskii–Moriya vector of CrX_3 as a function of the distance over the lattice constant (d/a). Temperature-dependence of magnetization (purple) and magnetic susceptibility (green) of $CrCl_3$ (**e**) without Dzyaloshinskii–Moriya interaction and (**f**) with Dzyaloshinskii–Moriya interaction. (For interpretation of the colors in the figure(s), the reader is referred to the web version of this article.)

finite DMI for this pair of atoms in the honeycomb lattice, even in a centrosymmetric material. This can be a new mechanism for realizing the skyrmion lattice in a centrosymmetric material, compared with the frustration and RKKY interaction proposed in previous studies [4–6]. In addition, it has been reported in the recent work of Wang et al. that the skyrmion phase can be stabilized in a honeycomb lattice model with a suitable ratio of the isotropic exchange coupling and the DMI value between the next-nearest neighbor [22]. The effect of the DMI on the magnetic properties of MX_3 (M: V, Cr, Mn, Fe; X: Cl, Br, I) cannot be neglected, and it can lead to rich magnetic properties. This motivated us to study the magnetic properties of these compounds considering the effect of the DMI, by combining first-principle calculations and Monte Carlo simulations.

In this workstudy, we derive the Hamiltonian from first-principle calculations, where the isotropic exchange, antisymmetric exchange (also known as the DMI), magnetic anisotropy, and the Zeeman term are considered. The Hamiltonian of the Heisenberg model is used as [23–25]

$$H_{\mathrm{Heis}} = -\sum_{<ij>} J_{ij}^{m}\overrightarrow{S_i}\cdot\overrightarrow{S_j} - \sum_{i} k_{\mathrm{u}}(\overrightarrow{e_u}\cdot\overrightarrow{S_i})^2 - \sum_{<ij>}\overrightarrow{D_{ij}}\cdot(\overrightarrow{S_i}\times\overrightarrow{S_j}) - g\mu_{\mathrm{B}}\sum_{i}\overrightarrow{H_{\mathrm{ext}}}\cdot\overrightarrow{S_i}, \quad (1)$$

where g is the g-factor, μ_{B} is the Bohr magneton, and k_{u} is the uniaxial anisotropy constant. The first term expresses the exchange interactions between the spins at sites i and j. The spin tends to be parallel to the neighboring site when the magnetic exchange coupling constant J_{ij}^{m} is positive, whereas the spin is antiparallel to the neighboring spin for negative J_{ij}^{m}. The magnetic exchange coupling constants can be calculated using the Liechtenstein formula with density functional theory (DFT) [26–28]. The values of the magnetic exchange coupling constants of the Cr–Cr pair of CrX_3 as a function of the distance over the lattice constant d/a are shown in Fig. 1c. The first nearest neighbor of the intralayer is a large positive value in all compounds, which can lead to a ferromagnetic order of the intralayer. The coupling constants of the first and second nearest neighbors of the interlayer in $CrCl_3$ are positive. This implies that the AFM order of the interlayer in the experimental work cannot be realized from the DFT results [29]. The second term in equation (1) indicates the interaction between the spin at site i and uniaxial anisotropy, and $\overrightarrow{e_u}$ is the direction of the easy axis in the case of a positive k_{u}. $\overrightarrow{e_u}$ is set to be out-of-plane (c direction), and k_{u} is evaluated from the value of the magnetocrystalline anisotropy energy (MAE) in first-principle calculations [30]. The MAE value in $CrCl_3$ is positive (0.034 meV/Cr–atom), and the easy axis is out-of-plane. This is again in contradiction with the in-plane easy plane in reported experimental works, which requires a negative MAE value [29]. The third term is the antisymmetric exchange term, with $\overrightarrow{D_{ij}}$ being the Dzyaloshinskii–Moriya vector, which can be calculated as the slope of the magnon at the Γ point in the case of spin spiral calculations [27,28,31]. The length of the Dzyaloshinskii–Moriya vector of the Cr–Cr pair of CrX_3 as a function of the distance over the lattice constant d/a is shown in Fig. 1d. The length of the Dzyaloshinskii–Moriya vector of the second nearest neighbor of the intralayer is quite large. In the case of CrI_3, the value of the second nearest neighbor is 0.33 meV, which is in agreement with the value extracted from the magnon spectrum in the experimental work [32,33]. In addition, the value for $CrCl_3$ is comparable to that for CrI_3, which can have a significant effect on the magnetic properties. We found that these comparable DMI values of $CrCl_3$ and CrI_3 are attributed to the spin-orbit coupling strength of X(X = Cl, I) and the hopping strength between Cr and X atoms. Specifically, according to the previous theoretical work [34,35], the magnitude of DMI value is controlled by the hopping strength between orbitals. The final term is the Zeeman term, which arises due owing to the effect of an external magnetic field on the spin.

The temperature dependence of the magnetization and magnetic susceptibility of $CrCl_3$ is shown in Fig. 1e–f. When the DMI is removed, $CrCl_3$ shows a clear normal magnetic transition from ferromagnetic to paramagnetic (FM–PM) in terms of magnetization and magnetic susceptibility. This means that the positive interlayer magnetic exchange coupling constants and positive MAE with the out-of-plane easy axis in $CrCl_3$ cannot support the in-plane AFM in the interlayer, as reported in previous experimental work, which required a negative exchange coupling constant of the interlayer and an in-plane MAE [29]. Subsequently, the effect of the DMI on the magnetization and magnetic susceptibility is considered. In the case of $CrCl_3$, the MAE (0.034 meV/Cr–atom) is significantly lower than that in the case of $CrBr_3$ (0.187 meV/Cr–atom) and CrI_3 (0.590 meV/Cr–atom), whereas its DMI is comparable to that of these compounds. This leads to the disappearance of FM as the ground state and the FM–PM transition in magnetization and magnetic susceptibility. The magnetization in the ground state is approximately equal to zero, and the magnetic susceptibility becomes negligible. It might have features similar to those of the AFM phase reported in experimental studies. This implies that the DMI is a critical factor in determining the ground state of $CrCl_3$. Although the FM phase is suppressed when the DMI is considered, magnetization appears with an applied magnetic field. Note that the FM–PM transition can survive in the CrI_3 and $CrBr_3$ cases even with the DMI, because their MAE is sufficiently strong to stabilize FM at low temperatures.

The magnetization of $CrCl_3$ as a function of temperature and an external magnetic field along the out-of-plane (c direction) with increasing field is shown in Fig. 2a. In a low external magnetic field and low-temperature region, the magnetization is approximately zero.

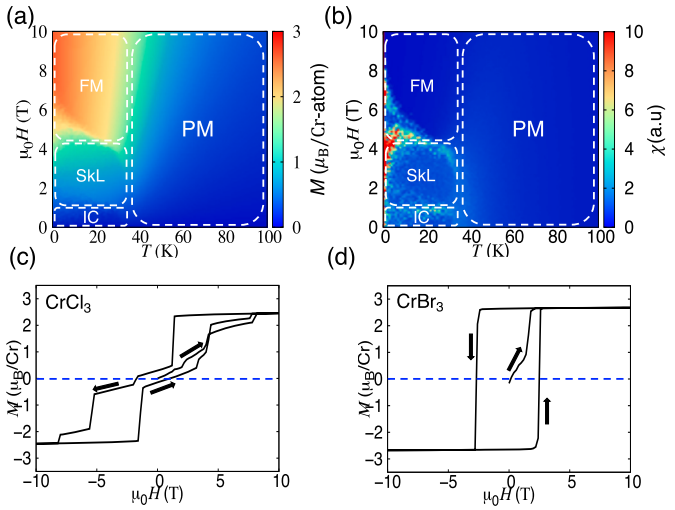

Fig. 2. (**a**) Magnetization of $CrCl_3$ as a function of temperature (horizontal axis) and an external magnetic field (vertical axis), where the magnetic field is along the out-of-plane (c direction) with increasing field. (**b**) Magnetic susceptibility of $CrCl_3$ as a function of temperature and an external magnetic field, where the magnetic field is along the out-of-plane (c direction) with increasing field. Hysteresis loops of (**c**) $CrCl_3$ and (**d**) $CrBr_3$ at 10 K and a low frequency of the field scan along c direction with the arrow indicate the path of magnetization curves.

When the magnetic field increases, the magnetization is enhanced and becomes spin-polarized with saturation of magnetization. The magnetic susceptibility as a function of the magnetization fluctuation is shown in Fig. 2b, where the magnetic field is along the out-of-plane (c direction) with increasing field. The boundary of the magnetic phase diagram can be identified by considering high magnetic susceptibility as a phase transition. The magnetic phase was examined by capturing a snapshot of the Monte Carlo simulation at equilibrium. Consequently, we found that at low temperatures and low magnetic fields, the magnetic phase is incommensurate, where the long-range spin texture is broken. When the external magnetic field is intermediate, the skyrmion lattice is stabilized, and when the external magnetic field is sufficiently large, spin polarization of the ferromagnetic state can occur. A snapshot of the skyrmions phase is presented in Fig. 3.

The magnetization versus magnetic field (M–H) curves, where magnetic field along c direction with the arrow indicates the path of magnetization curves, of $CrCl_3$ and $CrBr_3$ are shown in Fig. 2c–d, respectively. The hysteresis loop of $CrCl_3$, which shows a triangular shape with symmetry to the origin, is significantly different from the rectangular shape of the Stoner–Wohlfarth model, such as in the case of $CrBr_3$. An increase in the magnetic field can enhance magnetization and stabilize the FM phase. However, after realizing saturation magnetization, when the magnetic field decreases ~~to~~ close to zero, the magnetization decreases rapidly to zero. This phenomenon in the hysteresis loop is similar to that observed in the magnetization reversal process of a vortex. This peculiar behavior of the hysteresis loop is a fingerprint for the realization of the skyrmion phase in $CrCl_3$.

We found that the skyrmion phase also exists in the other MCl_3 materials. The magnetic exchange coupling constants and the Dzyaloshinskii–Moriya length of MCl_3 as a function of the distance over the lattice constants are shown in Fig. 3a–b, respectively. The first nearest neighbor of the magnetic exchange coupling constant of V–V, Cr–Cr, and Mn–Mn pairs is positive, whereas it is negative for Fe–Fe pairs. By contrast, the Dzyaloshinskii–Moriya vectors of VCl_3, $MnCl_3$, and $FeCl_3$ are comparable to that of $CrCl_3$, which is relatively large. Replacing Cl with Br and I can change the magnetic exchange coupling constants and the Dzyaloshinskii–Moriya lengths. The magnetocrystalline anisotropy energies of VCl_3, $MnCl_3$, and $FeCl_3$ were 0.023, −0.140, and 0.075 (meV/f.u), respectively. Only MCl_3 compounds are suitable for forming a skyrmion, because of their small MAE compared with DMI. The high MAE of the other compounds suppressed the effect of DMI on skyrmion formation. The magnetic susceptibility of VCl_3, which depends on the external magnetic field and temperature, and the magnetic field is along the out-of-plane (c direction) with increasing field, is shown in Fig. 3c. VCl_3 with small magnetic anisotropy and relatively high DMI, which is important for stabilizing the skyrmion lattice, yields a magnetic phase diagram similar to that of $CrCl_3$, as shown in Fig. 2b. It is noteworthy that the skyrmion lattice in VCl_3 can survive in a much larger external magnetic field than that in $CrCl_3$, although the Dzyaloshinskii–Moriya length is similar.

The in-plane components of the Dzyaloshinskii–Moriya vector for the second nearest neighbor of the intralayer of $CrCl_3$ and VCl_3 are shown in Fig. 3d. It is clear that the in-plane directions of the Dzyaloshinskii–Moriya vectors of $CrCl_3$ and VCl_3 are nearly opposite. This leads to different helicities of skyrmions with the Bloch-type, which is an additional degree of freedom. As the helicity of skyrmions is different when changing from $CrCl_3$ to VCl_3, it is possible to control the helicity of skyrmions through electric field-driven electron and hole doping. A snapshot of the Monte Carlo simulation of $CrCl_3$ and VCl_3 is shown in Fig. 3e–f. The skyrmion of $CrCl_3$ is Bloch clockwise, owing to the direction of the Dzyaloshinskii–Moriya vector. Further, the skyrmion of VCl_3 is also Bloch-type, with anticlockwise rotation of the spin. Owing to the non-vanishing of the Dzyaloshinskii–Moriya vector at the second nearest neighbor of the intralayer, the diameters of the skyrmions of both $CrCl_3$ and VCl_3 are small (approximately 2 nm), which is similar to the value in other centrosymmetric materials originating from frustration or RKKY interaction [4–6].

A snapshot of $MnCl_3$ at 1 K and zero external magnetic field is shown in Fig. 4a. The MAE value of $MnCl_3$ was −0.140 meV/(Mn atom) as the easy plane (ab plane). In this case, the meron, where the spin texture aligns in the in-plane of the skyrmion compared with out-of-plane of the skyrmion, can survive in $MnCl_3$ at zero external magnetic field, owing to the assistance of the in-plane MAE. This means that the meron in $MnCl_3$ does not require an external magnetic field as in the skyrmion case, which might reduce the power consumption to maintain the skyrmion lattice as $CrCl_3$ and VCl_3.

A snapshot of $FeCl_3$ at 1 K and zero external magnetic field is shown in Fig. 4b. $FeCl_3$ has a negative sign in the first and second nearest neighbors of the intralayer, and the highest Dzyaloshinskii–Moriya interactions among them are shown in Fig. 3a–b. It is important to stabilize antiferromagnetic (AFM) skyrmions, where the Hall effect is negligible compared with that in conventional skyrmions [36]. In this case, the AFM skyrmion is more convenient to use in a race track memory device without movement to the boundary of the Hall velocity in a conventional skyrmion. The strong negative of the first nearest neighbor can lead to the survival of AFM skyrmions above room temperature. However, it also leads to larger AFM skyrmions compared with conventional skyrmions such as $CrCl_3$ and VCl_3.

In summary, the magnetic properties of the van der Waals centrosymmetric MX_3 (M: V, Cr, Mn, Fe; X: Cl, Br, I) materials were studied by combining first-principle calculations with Monte Carlo simulations. The effect of the DMI, which is usually ignored in centrosymmetric lattices, was considered in this study. The DMI of the second nearest neighbor intralayer is non-negligible, which originates from the breaking of the local inversion symmetry. This is an indispensable factor in determining the magnetic properties of these compounds, such as the skyrmions in $CrCl_3$ and VCl_3. The small size of skyrmions in centrosymmetric materials is promising for spintronic applications, such as high-density magnetic memory devices. Conventional skyrmions ($CrCl_3$ and VCl_3) and antiferromagnetic skyrmions ($FeCl_3$) and merons in $MnCl_3$ were found in centrosymmetric materials in the present work. Our present work extends a new class of materials as a rare-earth free centrosymmetric lattice, where the skyrmion can exist because of the finite DMI.

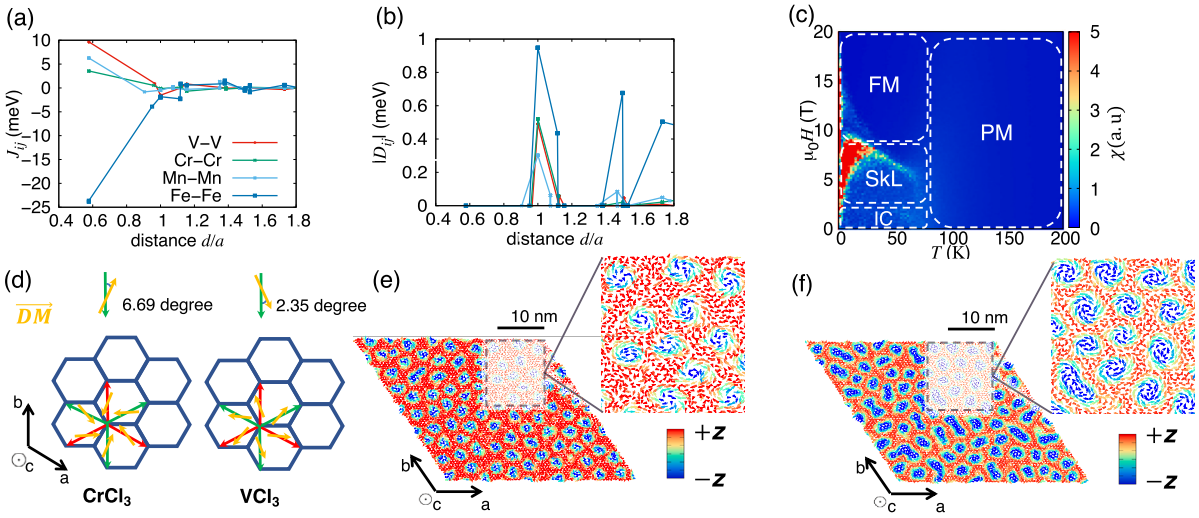

Fig. 3. (**a**) Magnetic exchange coupling constants of M–M pairs of MCl_3 (M: V, Cr, Mn, Fe) as a function of distance over lattice constant (d/a). (**b**) Length of Dzyaloshinskii–Moriya vector of MCl_3 as a function of distance over lattice constant (d/a). (**c**) Magnetic susceptibility of VCl_3 as a function of temperature and the external magnetic field, where the magnetic field is along the out-of-plane (c direction) with increasing field. (**d**) In-plane components of Dzyaloshinskii–Moriya vector for the second nearest neighbor of intralayer of $CrCl_3$ and VCl_3, where the red and green arrows indicate pairs with different sublattices, and the yellow arrow indicates the direction of Dzyaloshinskii–Moriya vector. (**e**) Snapshot of Monte Carlo simulation of $CrCl_3$ at 10 K with external magnetic field equal to 4 T along the positive z direction. (**f**) Snapshot of the Monte Carlo simulation of VCl_3 at 10 K with external magnetic field equal to 6 T along the positive z direction.

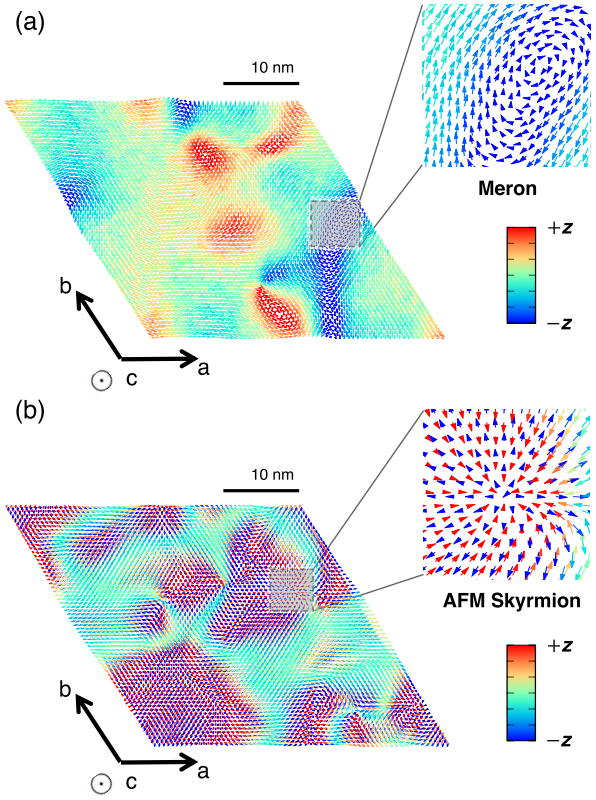

Fig. 4. (**a**) Snapshot of the Monte Carlo simulation of $MnCl_3$ at 1 K with zero external magnetic field. (**b**) Snapshot of the Monte Carlo simulation of $FeCl_3$ at 1 K with zero external magnetic field.

The relaxed crystal structure parameters and magnetocrystalline anisotropy energy were obtained using the VASP code with optB86b exchange functional as the van der Waals density functional [30,37]. The convergence of magnetocrystalline anisotropy energy was achieved using a number of k-point meshes of 18×18×6. The magnetic exchange coupling constants and Dzyaloshinskii–Moriya vectors were calculated based on the Green function multiple-scattering formalism, as implemented in the SPR–KKR code [26–28,31]. Monte Carlo simulations were performed using an in-house program using the Metropolis algorithm for the classical Heisenberg model [23–25]. The size of the cell in the Monte–Carlo simulation in MX_3 is 64×64×16-unit cells containing 393,216 magnetic atoms. The number of Monte–Carlo steps is 2,000,000, and the first 1,000,000 steps are discarded.

CRediT authorship contribution statement

H.B. Tran: Investigation, Writing – Original draft preparation. Y. Matsushita: Writing – Reviewing and Editing, Supervision.

Declaration of competing interest

The authors declare that they have no known competing financial interests or personal relationships that could have appeared to influence the work reported in this paper.

Data availability

The data that support the findings of this study are available from the corresponding author upon reasonable request.

Acknowledgements

The authors thank Prof. Tamio Oguchi and Dr. Kunihiko Yamauchi for their valuable discussions. This work was supported by MEXT via the “Program for Promoting Researches on the Supercomputer Fugaku” (JP-MXP1020200205) and JSPS KAKENHI via the “Grant-in-Aid for Scientific Research(A)” Grant Number 21H04553. The computation in this work was performed using the supercomputer Fugaku provided by the RIKEN Center for Computational Science, the Supercomputer Center at the Institute for Solid State Physics at the University of Tokyo, and the TSUBAME3.0 supercomputer at the Tokyo Institute of Technology.

References

[1] A. Fert, N. Reyren, V. Cros, Magnetic skyrmions: advances in physics and potential applications, Nat. Rev. Mater. 2 (2017) 17031.

[2] Y. Tokura, N. Kanazawa, Magnetic skyrmion materials, Chem. Rev. 121 (2021) 2857–2897.
[3] T. Moriya, Anisotropic superexchange interaction and weak ferromagnetism, Phys. Rev. 120 (1960) 91.
[4] T. Kurumaji, T. Nakajima, M. Hirschberger, A. Kikkawa, Y. Yamasaki, H. Sagayama, H. Nakao, Y. Taguchi, T. Arima, Y. Tokura, Skyrmion lattice with a giant topological Hall effect in a frustrated triangular-lattice magnet, Science 365 (2019) 914–918.
[5] N.D. Khanh, T. Nakajima, X. Yu, S. Gao, K. Shibata, M. Hirschberger, Y. Yamasaki, H. Segayama, H. Nakao, L. Peng, K. Nakajima, R. Takagi, T. Arima, Y. Tokura, S. Seki, Nanometric square skyrmion lattice in a centrosymmetric tetragonal magnet, Nat. Nanotechnol. 15 (2020) 444–449.
[6] R. Takagi, N. Matsuyama, V. Ukleev, L. Yu, J.S. White, S. Francoual, J.R.L. Mardegan, S. Hayami, H. Saito, K. Kaneko, K. Ohishi, Y. Onuki, T. Arima, Y. Tokura, T. Nakajima, S. Seki, Square and rhombic lattices of magnetic skyrmions in a centrosymmetric binary compound, Nat. Commun. 13 (2022) 1472.
[7] R. Yambe, R. Hayami, Skyrmion crystals in centrosymmetric itinerant magnets without horizontal mirror plane, Sci. Rep. 11 (2021) 11184.
[8] X. Yao, J. Chen, S. Dong, Controlling the helicity of magnetic skyrmions by electrical field in frustrated magnets, N. J. Phys. 22 (2020) 083032.
[9] C. Psaroudaki, C. Panagopoulos, Skyrmion qubits: a new class of quantum logic elements based on nanoscale magnetization, Phys. Rev. Lett. 127 (2021) 067201.
[10] J. Xia, X. Zhang, X. Liu, J. Zhou, M. Ezawa, Universal quantum computation based on nanoscale skyrmion helicity qubits in frustrated magnets, Phys. Rev. Lett. 130 (2022) 106701.
[11] K.M. Song, J.S. Jeong, B. Pan, X. Zhang, J. Xia, S. Cha, T.E. Park, K. Kim, S. Finizio, J. Raabe, J. Chang, Y. Zhou, W. Zhao, W. Kang, H. Ju, S. Woo, Skyrmion-based artificial synapses for neuromorphic computing, Nat. Electron. 3 (2020) 148–155.
[12] E.C. Ahn, 2D materials for spintronic devices, npj 2D Mater. Appl. 4 (2020) 17.
[13] M. Gibertini, M. Koperski, A.F. Morpurgo, K.S. Novoselov, Magnetic 2D materials and heterostructures, Nat. Nanotechnol. 14 (2019) 408–419.
[14] Y. Cao, V. Fatemi, S. Fang, K. Watanabe, T. Taniguchi, E. Kaxiras, J.H. Pablo, Unconventional superconductivity in magic-angle graphene superlattices, Nature 556 (2018) 43–50.
[15] T. Ando, Screening effect and impurity scattering in monolayer graphene, J. Phys. Soc. Jpn. 75 (2016) 074716.
[16] M. Koshino, N.F.Q. Yuan, T. Koretsune, M. Ochi, K. Kuroki, L. Fu, Maximally localized Wannier orbitals and the extended Hubbard model for twisted bilayer graphene, Phys. Rev. X 8 (2018) 031087.
[17] H. Nishi, Y. Matsushita, A. Oshiyama, Band-unfolding approach to Moiré-induced band-gap opening and Fermi level velocity reduction in twisted bilayer graphene, Phys. Rev. B 8 (2017) 085420.
[18] K. Uchida, S. Furuya, J. Iwata, A. Oshiyama, Atomic corrugation and electron localization due to Moiré patterns in twisted bilayer graphenes, Phys. Rev. B 90 (2014) 155451.
[19] M.S. Dresselhaus, A. Jorio, M. Hofmann, G. Dresselhaus, R. Saito, Perspectives on carbon nanotubes and graphene Raman spectroscopy, Nano Lett. 10 (2010) 751–758.
[20] M.A. McGuire, Crystal and magnetic structures in layered, transition metal dihalides and trihalides, Crystals 7 (2017) 121.
[21] L.L. Handy, N.W. Gregory, Structural properties of chromium(III) iodide and some chromium(III) mixed halides, J. Am. Chem. Soc. 74 (1952) 891–893.
[22] W. Wang, J. Sun, H. Li, Stabilization of skyrmions in two-dimensional systems with next-nearest-neighbor exchange interactions, Front. Phys. 10 (2022) 995902.
[23] H.B. Tran, H. Momida, Y. Matsushita, K. Sato, Y. Makino, K. Shirai, T. Oguchi, Effect of magnetocrystalline anisotropy on magnetocaloric properties of an AlFe_2B_2 compound, Phys. Rev. B 105 (2022) 134402.
[24] H.B. Tran, H. Momida, Y. Matsushita, K. Shirai, T. Oguchi, Insight into anisotropic magnetocaloric effect of CrI_3, Acta Mater. 231 (2022) 117851.
[25] H.B. Tran, Y. Matsushita, Dzyaloshinskii–Moriya interactions in Nd_2Fe_14B as the origin of spin reorientation and the rotating magnetocaloric effect, Appl. Mater. Today 32 (2023) 101825.
[26] A.I. Liechtenstein, M.I. Katsnelson, V.P. Antropov, V.A. Gubanov, Local spin density functional approach to the theory of exchange interactions in ferromagnetic metals and alloys, J. Magn. Magn. Mater. 67 (1987) 65–74.
[27] H. Ebert et al., The Munich SPR-KKR package, version 7.7.
[28] H. Ebert, D. Ködderitzsch, J. Minár, Calculating condensed matter properties using the KKR-Green's function method-recent developments and applications, Rep. Prog. Phys. 74 (2011) 096501.
[29] M.A. McGuire, G. Clark, K.C. Santosh, W.M. Chance, G.E. Jellison, V.R. Cooper, X. Xu, B.C. Sales, Magnetic behavior and spin-lattice coupling in cleavable van der Waals layered CrCl_3 crystals, Phys. Rev. Mater. 1 (2017) 014001.
[30] G. Kresse, J. Furthmüller, Efficient iterative schemes for *ab initio* total-energy calculations using a plane-wave basis set, Phys. Rev. B 54 (1996) 11169–11186.
[31] S. Mankovsky, H. Ebert, Accurate scheme to calculate the interatomic Dzyaloshinskii-Moriya interaction parameters, Phys. Rev. B 96 (2017) 104416.
[32] L. Chen, J.H. Chung, B. Gao, T. Chen, M.B. Stone, A.I. Kolesnikov, Q. Huang, P. Dai, Topological spin excitations in honeycomb ferromagnet CrI_3, Phys. Rev. X 8 (2018) 041028.
[33] L. Chen, J.H. Chung, M.B. Stone, A.I. Kolesnikov, B. Winn, V.O. Garlea, D.L. Abernathy, B. Gao, M. Augustin, Elton.J.G. Santos, P. Dai, Magnetic field effect on topological spin excitations in CrI_3, Phys. Rev. X 11 (2021) 031047.
[34] G. Beutier, S.P. Collins, O.V. Dimitrova, V.E. Dmitrienko, M.I. Katsnelson, Y.O. Kvashnin, A.I. Liechtenstein, V.V. Mazurenko, A.G.A. Nisbet, E.N. Ovchinnikova, D. Pincini, Band filling control of the Dzyaloshinskii-Moriya interaction in weakly ferromagnetic insulators, Phys. Rev. Lett. 119 (2017) 167201.
[35] J. Chang, J. Zhao, Y. Ding, Anisotropic superexchange through nonmagnetic anions with spin-orbit coupling, Eur. Phys. J. B 93 (2020) 159.
[36] X. Zhang, Y. Zhou, M. Ezawa, Antiferromagnetic skyrmion: stability, creation and manipulation, Sci. Rep. 6 (2016) 24795.
[37] J. Klimeš, D.R. Bowler, A. Michaelides, Van der Waals density functionals applied to solids, Phys. Rev. B 83 (2011) 195131.